

## Supporting Information

### Systematic Evaluation of Structure-Property Relationships in Heteroacene - Diketopyrrolopyrrole Molecular Donors for Organic Solar Cells

Stephen Loser, Sylvia J. Lou, Brett M. Savoie, Carson J. Bruns, Amod Timalsina, Matthew J. Leonardi, Jeremy N. Smith, Tobias Harschneck, Riccardo Turrisi, Nanjia Zhou, Charlotte L. Stern, Amy A. Sarjeant, Antonio Facchetti,\* Robert P. H. Chang,\* Samuel I. Stupp,\* Mark A. Ratner,\* Lin X. Chen\* and Tobin J. Marks\*

#### Experimental

*Synthesis.* The small-molecule donors were synthesized by Stille cross coupling of the appropriate stannylated heterocyclic acenes with TDPPBr in good yields (80%-91%) according to established methodologies (Scheme 1).<sup>1, 2</sup> Synthetic procedures for **BDT**, **NDT**, and **zNDT** have been previously published.<sup>1-3</sup> **BDF** was synthesized by adding Pd(PPh<sub>3</sub>)<sub>4</sub> (85 mg, 74 μmol) to a degassed mixture of TDPPBr (702 mg, 1.16 mmol) and 1,5-bis(trimethylstannyl)-4,8-bis((2-ethylhexyl)oxy)benzo[1,2-*b*:4,5-*b'*]difuran (344 mg, 0.465 mmol) in 6:1 PhMe:DMF (7 mL) and heated to 110 °C under N<sub>2</sub> for 20 h. The solution was added to MeOH (100 mL) and the resulting precipitate was collected by filtration and chromatographed on SiO<sub>2</sub> (hexanes:CHCl<sub>3</sub> 1:2) to afford a dark purple solid. Recrystallization in CHCl<sub>3</sub> by slow vapor diffusion of EtOAc afforded **BDF** as tiny crystalline needles (426 mg, 63%). <sup>1</sup>H NMR (CDCl<sub>3</sub>, 298 K, 500 MHz) δ = 9.05 (d, *J* = 4.0 Hz, 2H), 8.94 (d, *J* = 4.0 Hz, 2H), 7.65 (d, *J* = 5.0 Hz, 2H), 7.60 (d, *J* = 4.0 Hz, 2H), 7.29 (dd, *J* = 4.0, 5.0 Hz, 2H), 7.20 (s, 2H), 4.45 (d, *J* = 5.5 Hz, 4H), 4.13–4.02 (m, 8H), 1.96 (hep, *J* = 6.5 Hz, 2H), 1.89 (hep, *J* = 6.5 Hz, 2H), 1.83 (hep, *J* = 6.0 Hz, 2H), 1.72–1.48 (m, 8H), 1.46–1.23 (m, 40H), 1.05 (t, *J* = 7.5 Hz, 6H), 0.95 (t, *J* = 7.0 Hz, 6H), 0.94 (t, *J* = 7.5 Hz, 6H), 0.90 (t, *J* = 7.5 Hz, 6H), 0.88 (t, *J* = 7.0 Hz, 6H), 0.87 (t, *J* = 7.5 Hz, 6H). <sup>13</sup>C (CDCl<sub>3</sub>, 298 K, 125 MHz) δ = 161.9, 161.8, 149.7, 142.3, 140.4, 139.8, 137.8,

136.8, 135.6, 131.1, 130.8, 130.0, 129.6, 128.6, 125.6, 122.3, 108.7, 108.3, 102.4, 75.9, 46.1, 46.1, 40.3, 39.3, 39.2, 30.5, 30.3, 29.3, 28.5, 28.5, 23.9, 23.7, 23.7, 23.3, 23.2, 14.4, 14.2, 14.2, 11.4, 10.6. HRMS (MMI-TOF-MS)  $m/z$  calcd for  $C_{86}H_{115}N_4O_8S_4$  [ $M + H$ ]<sup>+</sup>: 1459.7593, found 1459.7637. Anal. Calcd for  $C_{86}H_{114}N_4O_8S_4$ : C, 70.74; H, 7.87; N, 3.84. Found: C, 70.97; H, 7.91; N, 3.80.

To synthesize **aBDT**, Pd(PPh<sub>3</sub>)<sub>4</sub> (40 mg, 0.03 mmol) was added to a degassed solution of 1-trimethylstannyl-4,8-bis((2-ethylhexyl)oxy)benzo[1,2-*b*:4,5-*b'*]dithiophene (280 mg, 0.38 mmol) and TDPPBr (200 mg, 0.33 mmol) in 4:1 PhMe:DMF (3.5 mL) and heated to 110 °C for 16 h. The reaction mixture was next cooled to ambient temperature and poured into 25 mL MeOH. The resulting precipitate was then collected by vacuum filtration and chromatographed on silica (1:1 CH<sub>2</sub>Cl<sub>2</sub>:hexanes) to afford a purple solid (291 mg, 91%). <sup>1</sup>H NMR (CDCl<sub>3</sub>, 500 MHz, 298 K)  $\delta$  = 9.01 (d,  $J$  = 4.1 Hz, 1H), 8.93 (dd,  $J$  = 3.9, 1.2 Hz, 1H), 7.67 (s, 1H), 7.65 (dd,  $J$  = 4.9, 1.2 Hz, 1H), 7.48 (d,  $J$  = 5.5 Hz, 1H), 7.46 (d,  $J$  = 4.2 Hz, 1H), 7.41 (d,  $J$  = 5.5 Hz, 1H), 7.29 (d,  $J$  = 5.0, 3.9 Hz, 1H), 4.22 (d,  $J$  = 5.6 Hz, 2H), 4.19 (d,  $J$  = 5.5 Hz, 2H), 4.11–4.02 (m, 4H), 1.96 (hep,  $J$  = 6.7 Hz, 1H), 1.89 (hep,  $J$  = 6.7 Hz, 1H), 1.89–1.80 (m, 2H), 1.75–1.50 (m, 6H), 1.44–1.23 (m, 26H), 1.05 (t,  $J$  = 7.5 Hz, 3H), 1.04 (t,  $J$  = 7.5 Hz, 3H), 0.98–0.93 (m, 9H), 0.91–0.86 (m, 9H). <sup>13</sup>C (CDCl<sub>3</sub>, 125 MHz, 298K)  $\delta$  = 161.7, 161.6, 145.0, 144.2, 142.6, 140.3, 139.7, 136.8, 135.4, 135.0, 132.5, 131.8, 130.6, 130.5, 129.8, 129.2, 129.0, 128.5, 126.6, 126.2, 120.4, 117.7, 108.4, 108.1, 76.2, 76.1, 45.9, 40.6, 40.6, 39.2, 39.1, 30.4, 30.4, 29.2, 28.4, 28.3, 23.8, 23.6, 23.5, 23.1, 23.1, 14.2, 14.1, 14.1, 11.3, 11.3, 10.5, 10.5. HRMS (ESI-TOF-MS):  $m/z$  calcd for  $C_{56}H_{77}N_2O_4S_4$  [ $M + H$ ]<sup>+</sup> 969.4761, found 969.4744.

*Optical Absorption Spectroscopy.* Optical spectra were acquired on a Varian Cary 5000 UV-Vis-NIR spectrophotometer. Serial dilution was performed for each sample to determine the molar extinction coefficients in chloroform solution. Active layers were spun-cast on glass slides from chloroform solution and film thicknesses were measured by profilometry with a Veeco Dektak 150 surface profilometer. The absorption coefficients in films were determined by scaling the absorption by film thickness.

*Cyclic Voltammetry (CV).* CV on the donor compounds was performed in CH<sub>2</sub>Cl<sub>2</sub> solution at a concentration of 0.25 mg·mL<sup>-1</sup> using 0.1 M NBu<sub>4</sub>PF<sub>6</sub> as electrolyte (recrystallized from EtOH) on a Epsilon-C3 system (Bioanalytical Systems). The electrochemical cell was equipped with a Pt wire, Ag wire, and a glassy carbon (3 mm<sup>2</sup>) electrode which were used as the counter electrode, the pseudo-reference, and working electrode, respectively. All scan rates were 100 mV·s<sup>-1</sup> and the solutions were purged with CH<sub>2</sub>Cl<sub>2</sub>-saturated N<sub>2</sub> prior to use. Ferrocene was purified by sublimation for the ferrocene/ferrocenium (Fc/Fc<sup>+</sup>) redox couple and was used as the internal standard, and assigned an energy level of -4.88 eV vs. vacuum.

*Differential Scanning Calorimetry (DSC).* DSC data were collected on an In-calibrated Mettler-Toledo DSC822e instrument equipped with a TSO801RO autosampler. The samples (weight range 1.5 - 3.0 mg) were placed in lidded 30 μL Al pans and thermally cycled twice under N<sub>2</sub> with a heating rate of 10 °C per min and a slower cooling rate of 5 °C per min to minimize overcooling effects. The reported cycles correspond to the second cycle and are all plotted exotherm up/endothrm down.

*Single Crystal Growth and Characterization:* Single crystals suitable for X-ray diffraction were grown by slow evaporation of anhydrous CHCl<sub>3</sub> solutions. Prior to

crystal growth  $\sim 1 \text{ mg}\cdot\text{mL}^{-1}$  solutions of each compound were filtered through a  $0.22 \text{ }\mu\text{m}$  PTFE syringe filter and placed in clean vials equipped with tight-fitting caps with pierced rubber septa for slow solvent evaporation. Crystals were mounted in inert oil, and transferred to the cold gas stream of a Bruker Apex-II equipped with either synchrotron radiation from the Advanced Photon Source (APS) at Argonne National Laboratory or a  $\text{CuK}\alpha$  radiation source at the Integrated Molecular Structure Education and Research Center (IMSERC) of Northwestern University. SADABS was used for absorption correction of the **BDT**, **BDF**, and **aBDT** crystals, and SAINTPLUS for the **NDT** crystal.

*Film Grazing Incidence X-ray Scattering.* Grazing incidence X-ray scattering (GIXS) was performed at Beamline 8ID at the Advanced Photon Source (APS) at Argonne National Laboratory. Thin films of the active layer were spun-cast on  $\text{Si/SiO}_2$  wafers under the same conditions used for OPVs. Films were illuminated with a  $7.35 \text{ keV}$  ( $\lambda = 1.6868 \text{ nm}$ ) X-ray beam at an incident angle of  $0.19^\circ$ . Exposure times were varied between 10 and 30 s and the scattered X-ray beam, described by the scattering vector  $q$ , was collected on a Pilatus detector located 204 mm from the sample. The scattering vector  $q = 4\pi\sin(\theta)/\lambda$ , where  $\theta$  is the angle of scatter and  $q$  is inversely proportional to the  $d$ -spacing of a given diffraction plane,  $q = 2\pi/d$ . Data were normalized by exposure time.

Scherrer analysis was used to relate the peak width of a given diffraction spot associated with a Bragg plane to the crystalline correlation length, or the crystalline domain size, perpendicular to the given plane. The Scherrer equation is given in eq. 1,

$$D_{hkl} = \frac{2\pi K}{(\Delta q_{hkl})} \quad (1)$$

where  $K$  is the Scherrer constant related to the domain shape,  $\Delta q_{hkl}$  is the full-width half maximum of the peak associated with Bragg reflection ( $hkl$ ), and  $D_{hkl}$  is the crystalline domain size perpendicular to plane ( $hkl$ ). A corrected  $\Delta q_{hkl}$  was used to account for instrumental resolution and  $K = 0.9$  for spherical organic domains.<sup>4</sup> Note that the Scherrer analysis calculates a minimum domain size and does not account for degree of crystallinity, so a narrower peak can be attributed to either an increase in domain size or an increase in crystalline order.

*Electronic Structure Calculations:* The intermolecular electronic couplings relevant to hole transfer were calculated using geometries derived from the experimental crystal structures and a fragment based DFT calculation. The charge transfer integrals between HOMO orbitals on each molecule were calculated at the B3LYP/ADZP level of theory using the Amsterdam Density Functional (ADF) software package. Here ADZP is an augmented double-zeta polarizable basis set specifically developed for ADF's architecture. In the calculation, Kohn-Sham orbitals calculated for each molecule in isolation are used to evaluate the charge transfer integral between pairs of molecules.

The internal reorganization energy,  $\lambda_i$ , was calculated from the standard definition based on the Marcus reaction coordinates.<sup>5, 6</sup> In the case of cation self-exchange between identical subunits, this takes the form of eq. 2,

$$\lambda_i = E_+(0) + E_0(+) - E_+(+) - E_0(0) \quad (2)$$

where + and 0 refer to the cation and neutral species, subscripts refer to the electronic configuration, and parentheses refer to the geometric configurations (e.g.,  $E_+(0)$  refers to the total energy of the donor cation in the optimized neutral geometry). To evaluate the four energies in eq. 2, geometry optimizations of each donor cation and neutral species

were first carried out at the B3LYP/6-31G\* level using frequency analysis to confirm the minima. Single point calculations on these geometries, in each electronic configuration, were performed to obtain the terms in eq. 2.

Optical bandgap energies were computed from time-dependent density functional theory (TD-DFT) at the B3LYP/6-31G\* level on the optimized neutral geometry of each donor. The first singlet excitation of non-zero oscillator strength is reported. HOMO energies were obtained from the single point calculations on the optimized neutral geometries of each donor. HOMO energies are used here as approximations of the diabatic (vertical) ionization potential of each donor for comparison with electrochemistry. All geometry optimizations, single point calculations, and TD-DFT calculations were performed with QCHEM 4.0.<sup>7</sup>

*Organic Field Effect Transistor Fabrication:* Bottom-gate/top-contact OFETs were fabricated on p<sup>+</sup>-Si/SiO<sub>2</sub> (300 nm thermal oxide; Montco Silicon Technologies Inc.) coated with an octadecyltrichlorosilane (OTS) self-assembled monolayer to afford an advancing aqueous contact angle of 102°–103°. The molecular semiconductor concentration was 5 mg·mL<sup>-1</sup> and all solutions were filtered through a 0.45 μm PTFE membrane prior to spin-coating. Semiconductors were spun-cast at 1500 rpm for 30 s and then annealed at various temperatures under N<sub>2</sub>. Gold source/drain electrodes were then thermally evaporated through a shadow mask (W = 5000, L = 100 μm) to afford a final device structure, Si/SiO<sub>2</sub>/molecule/Au.

*Space Charge Limited Current (SCLC) Single Carrier Diode Fabrication:* Hole-only diodes were fabricated on ITO coated glass with a PEDOT:PSS bottom contact and a MoO<sub>3</sub>/Au top contact (2–3 nm MoO<sub>3</sub>; 50 nm Au). The top contact was the injecting

electrode and device areas ( $A$ ) were  $200 \times 200 \mu\text{m}^2$ . The current density,  $J$ , as a function of applied macroscopic electric field,  $E$ , displayed both Ohmic and space charge limited regimes. The latter was fit using the model of eq. 3 to extract the zero-field mobility,  $\mu_0$ , and the field dependence coefficient,  $\gamma$ ,

$$J = \frac{9}{8} \frac{\epsilon_s}{L} E^2 \mu_0 \exp(0.89\gamma\sqrt{E}) \quad (3)$$

where  $\epsilon_s$  and  $L$  are the semiconductor permittivity (taken as  $3\epsilon_0$ ) and thickness, respectively. Film thicknesses were 130–190 nm for the neat materials and 200–230 nm for the blends. Averages were taken over four separate devices. The Ohmic regime was also fit with a low-field carrier density,  $n_0$ , using eq. 4, and the applied voltage was corrected for the series resistance of the ITO ( $10 \Omega$ ; eq. 5).

$$J = n_0 e \mu_0 E \quad (4)$$

$$E = \frac{V_{\text{applied}} - J A R_{\text{series}}}{L} \quad (5)$$

Devices were measured in the dark in vacuo using an Agilent B1500A semiconductor parameter analyzer.

*Organic Photovoltaic (OPV) Cell Fabrication and Characterization:* Pre-patterned ITO-coated glass (Thin Film Device, Inc.) with a resistivity of  $<10\Omega$  and thickness of 280 nm was cleaned by sequential sonications at  $50^\circ\text{C}$  in soap/DI water, DI water, methanol, isopropanol, and acetone for 30 min each. ITO substrates were next treated for 5 min in an  $\text{O}_2$  plasma cleaner at 100 mTorr (Harrick Plasma). PEDOT:PSS (Clevios P VP Al 4083) was then spun-cast at 5000 rpm for 30 s on them and subsequently annealed at  $150^\circ\text{C}$  for 15 min. Samples were then transferred to a  $\text{N}_2$ -filled glove box for active layer and

top contact deposition. Active layers containing the donor molecules and the PCBM acceptor (>99.5% pure, American Dye Source) were formulated inside the glove box in a 1.5:1.0 (w:w) ratio at a molecule concentration of  $7 \text{ mg}\cdot\text{mL}^{-1}$  in anhydrous chloroform ( $\text{CHCl}_3$ ). Active layer solutions were stirred at 600 – 800 rpm for 1.5 h at  $50^\circ\text{C}$ , then spun-cast at 4000 rpm for 15 s to afford an active layer thickness of  $\sim 70 \text{ nm}$  by profilometry. Samples were then thermally annealed between  $70\text{--}130^\circ\text{C}$  for 10 min on a temperature-controlled hot plate. To complete device fabrication, LiF(1.0 nm)/Al(100 nm) were thermally evaporated, sequentially, at a base pressure of  $\sim 2.0 \times 10^{-6}$  Torr. The top Al electrodes were finally encapsulated with UV-curable epoxy and a glass slide before device evaluation. Each substrate contained 4 pixels with a defined area of  $0.065 \text{ cm}^2$  each.

OPV characterization was performed on a Spectra-Nova Class A Solar Simulator with AM1.5G light ( $100 \text{ mW}/\text{cm}^2$ ) from a Xe arc lamp. The light source was calibrated with an NREL-certified Si diode equipped with a KG3 filter to bring spectral mismatch to unity. Current vs. potential ( $J$ - $V$ ) measurements were recorded with a Keithly 2400 digital source meter. External quantum efficiency (EQE) measurements were performed using an Oriel Model S2QE-PV-SI (Newport Instruments) equipped with a NIST-certified Si diode, a Merlin lock-in amplifier, an optical chopper, and a 300 W Xe arc lamp.

#### *Single crystal x-ray diffraction*

Single crystals of  $\text{BDT}(\text{TDPP})_2$  were recrystallized from anhydrous chloroform, mounted in inert oil, and transferred to the cold gas stream of a Bruker D8 goniometer with APEXII CCD detector equipped with a synchrotron with Silicon (111)&(311). SADABS-2008/1 (Bruker, 2008) was used for absorption correction.

Single crystals of BDF(TDPP)<sub>2</sub> were recrystallized from anhydrous chloroform, mounted in inert oil, and transferred to the cold gas stream of a Bruker Apex2 equipped with a synchrotron with Silicon (111). SADABS-2012/1 (Bruker, 2012) was used for absorption correction.

Single crystals of BDTTDPP were recrystallized from CHCl<sub>3</sub>/EtOAc, mounted in inert oil, and transferred to the cold gas stream of a Bruker Kappa APEX CCD area detector equipped with a CuK $\alpha$  microsource with MX optics. SADABS-2008/1 (Bruker, 2008) was used for absorption correction.

A brown needle crystal of NDT(TDPP)<sub>2</sub> having approximate dimensions of 0.43 x 0.02 x 0.02 mm was mounted using oil (Infineum V8512) on a glass fiber. All measurements were made on a Bruker APEX-II CCD Diffractometer with a CuK $\alpha$  IuS source. Data were collected using Bruker APEX2 detector and processed using SAINTPLUS from Bruker.

**Table S1. Unit cell parameters and structure solution details**

Compound	BDTTDPP	BDT(TDPP) <sub>2</sub>	BDF(TDPP) <sub>2</sub>	NDT(TDPP) <sub>2</sub>
Empirical formula	C <sub>56</sub> H <sub>76</sub> N <sub>2</sub> O <sub>4</sub> S <sub>4</sub>	C <sub>86</sub> H <sub>114</sub> N <sub>4</sub> O <sub>6</sub> S <sub>6</sub>	C <sub>86</sub> H <sub>114</sub> N <sub>4</sub> O <sub>8</sub> S <sub>4</sub>	C <sub>90</sub> H <sub>116</sub> N <sub>4</sub> O <sub>6</sub> S <sub>6</sub>
Temperature (K)	100.01	100.15	100	100 (2)
Morphology	Needle	Needle	Needle	Needle
Color	purple	brown	brown	brown
Crystal system	Monoclinic	Monoclinic	Monoclinic	Triclinic
Space group	P 2 <sub>1</sub> /c	C 2/c	C 2/c	P -1
a (Å)	15.2482(3)	33.287(11)	33.795 (2)	6.3929(5)
b (Å)	10.0758(2)	5.6052(19)	5.449(3)	17.4732(13)
c (Å)	34.5945(8)	45.613(15)	45.61(2)	18.4977(15)
$\alpha$ (°)	90	90	90	90.241(6)
$\beta$ (°)	97.579(2)	10.234(5)	111.75	93.609(6)
$\gamma$ (°)	90	90	90	97.132(6)
Molecular length (Å)	19.380	31.807	31.361	34.417

Z	4	4	4	1
Density (g/cm <sup>3</sup> )	1.222	1.241	1.243	1.252
Volume (Å <sup>3</sup> )	5268.59	7985.32	7787.45	2046.07
Void space (%)	2.9	11.3	6.8	4.6
R1 (%)	15.90	25.87	22.14	9.32
wR2 (%)	34.20	52.78	41.58	25.79
GOF	1.177	2.098	1.470	1.083

Comparison of single crystal structure and film crystal structure

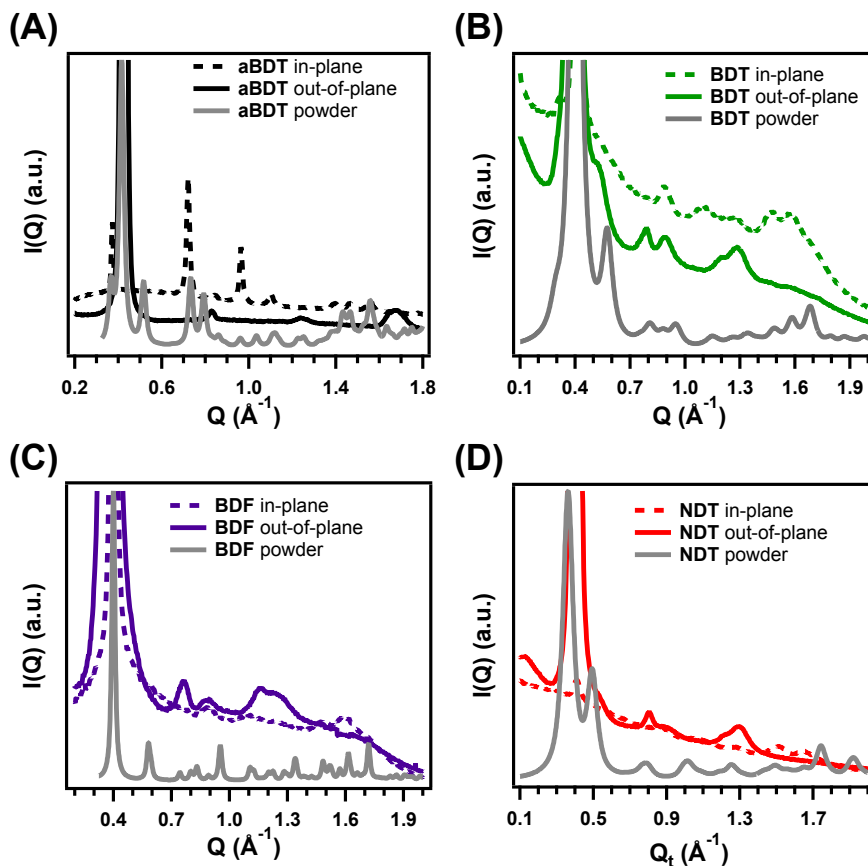


**Figure S1.** Comparison of powder diffraction calculated from the single crystal structure and data showing in-plane and out-of-plane structure from GIWAXS.

**Table S2. Comparison of peaks from calculated powder diffraction and GIWAXS.**

<sup>a</sup>Denotes peaks used to measure the lamellar  $d$ -spacing in thin film and <sup>b</sup>denotes peaks used to measure the  $\pi$ - $\pi$   $d$ -spacing in thin film. Peaks along the  $q_z$  axis are noted in bold.

BDTTDPP		
$hkl$	Powder	GIWAXS
$(002)^a$	0.37	0.37
$(100)$	0.42	<b>0.43</b>
$(10-2)$	0.52	NA
$(103)$	0.73	0.72

(10-4)	0.79	<b>0.83</b>
(201)	0.86	0.84
(113)	0.96	0.96
(210)	1.04	NA
(10-6)	1.12	1.10
(30-2)	1.23	NA
(020)	1.25	<b>1.24</b>
(311)		
(21-6)	1.43	1.40
(10-8)		
(008) <sup>b</sup>	1.47	1.46
(22-3)	1.56	1.56
(125)	1.63	1.66, <b>1.67</b>
(223)	1.71	NA
(315)	1.76	NA
(225)	1.81	1.78

BDT(TDPP) <sub>2</sub>		
<i>hkl</i>	Powder	GIWAXS
(020) <sup>a</sup>	0.40	0.39, <b>0.37</b>
(200)	0.58	<b>0.51</b>
(004)		
(202)	0.75	<b>0.77</b>
(400)	0.81	NA
(006)	0.88	0.88, <b>0.89</b>
(40-6)		
(402)	0.95	NA
(404)		
(60-4)		
(60-2)	1.15	1.10, <b>1.17</b>
(113)	1.24	1.27, <b>1.27</b>
(312)		
(602)	1.35	1.39
(116)	1.49	1.48
(117) <sup>b</sup>		
(11-8)	1.59	1.59
(118)	1.68	1.68

BDF(TDPP) <sub>2</sub>		
<i>hkl</i>	Powder	GIWAXS
(200) <sup>a</sup>	0.40	0.40, <b>0.37</b>
(005)	0.58	NA
(40-2)	0.74	<b>0.76</b>
(40-4)	0.80	NA

(400)	0.83	NA
(20-6) (204)	0.89	<b>0.89, 0.91</b>
(402) (40-6)	0.95	NA
(20-8) (206)	1.11	1.11
(60-4) (60-2)	1.13	<b>1.17</b>
(600) (60-6)	1.20	NA
(11-3)	1.23	<b>1.25, 1.27</b>
(602)	1.34	NA
(80-4) (51-2) <sup>b</sup> (51-3)	1.48	<b>1.48, 1.43</b>
(51-5) (314) (80-2)	1.52	NA
(31-5)	1.57	NA
(117)	1.62	1.60

NDT(TDPP) <sub>2</sub>		
<i>hkl</i>	Powder	GIWAXS
(001) <sup>a</sup> (010)	0.36	<b>0.40, 0.38</b>
(011) (01-1)	0.49	<b>0.53</b>
(012) (021)	0.78	<b>0.85, 0.78, 0.88</b>
(003)	1.02	1.06
(1-2-1)	1.22	<b>1.18</b>
(03-2) (023) (1-12) (102)	1.25	<b>1.28, 1.28</b>
(1-13) (03-3) (041) (033) (1-2-3)	1.50	1.50
(1-40) <sup>b</sup> (1-1-4)	1.65	1.64

*Determination of preferential orientation in neat and blend films*

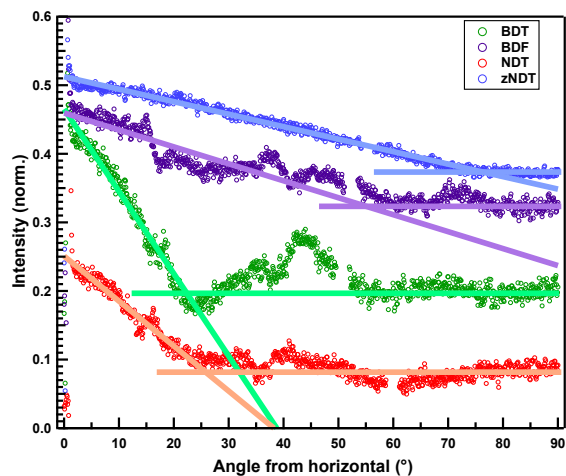


**Figure S2.** Fitting the circular linecuts of the  $\pi$ - $\pi$  stacking peak in neat films to determine degree of preferential orientation.

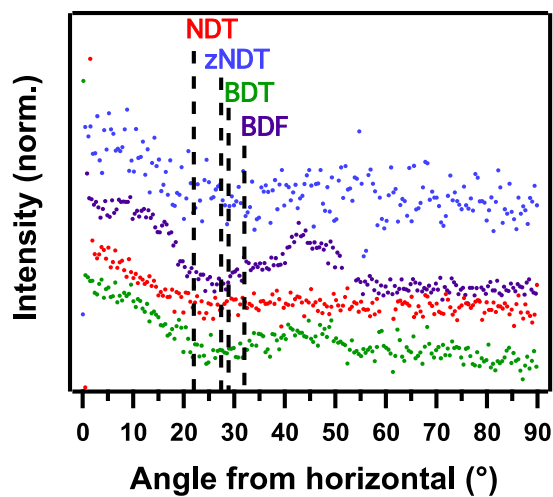


**Figure S3.** Circular linecuts of the  $\pi$ - $\pi$  stacking peak in blend films. *Calculated molecular orbitals and energies*

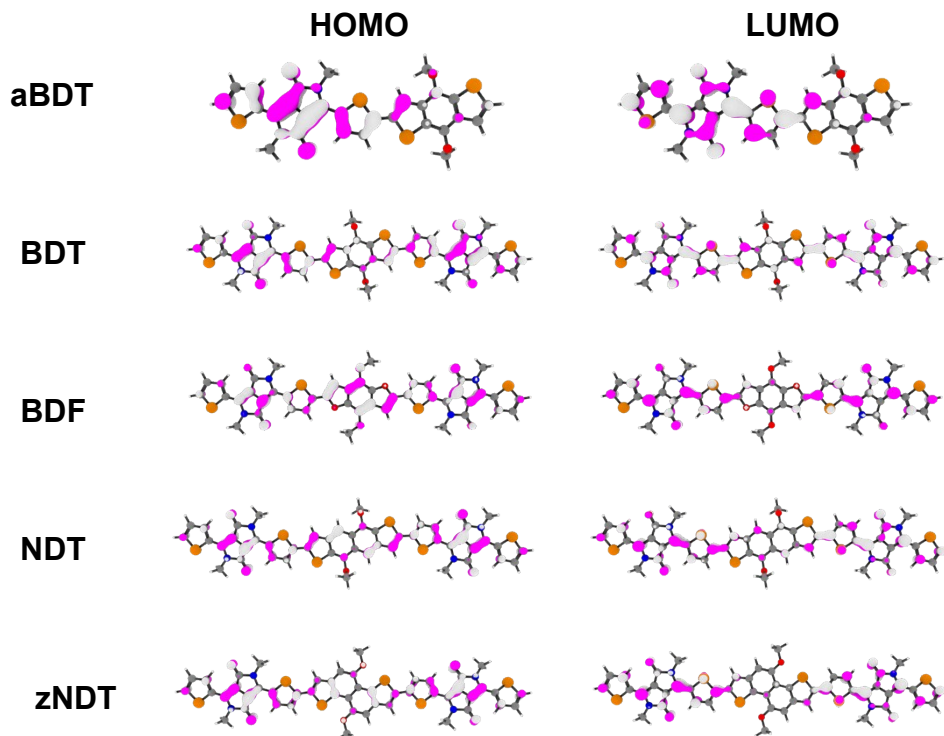


**Figure S4.** Calculated molecular orbitals

**Table S3.** Calculated HOMO energies

Compound	BDTTDPP	BDT(TDPP) <sub>2</sub>	BDF(TDPP) <sub>2</sub>	NDT(TDPP) <sub>2</sub>	zNDT(TDPP) <sub>2</sub>
HOMO (eV)	-4.90	-4.84	-4.71	-4.84	-4.73

*OFET and SCLC Mobility Measurements*

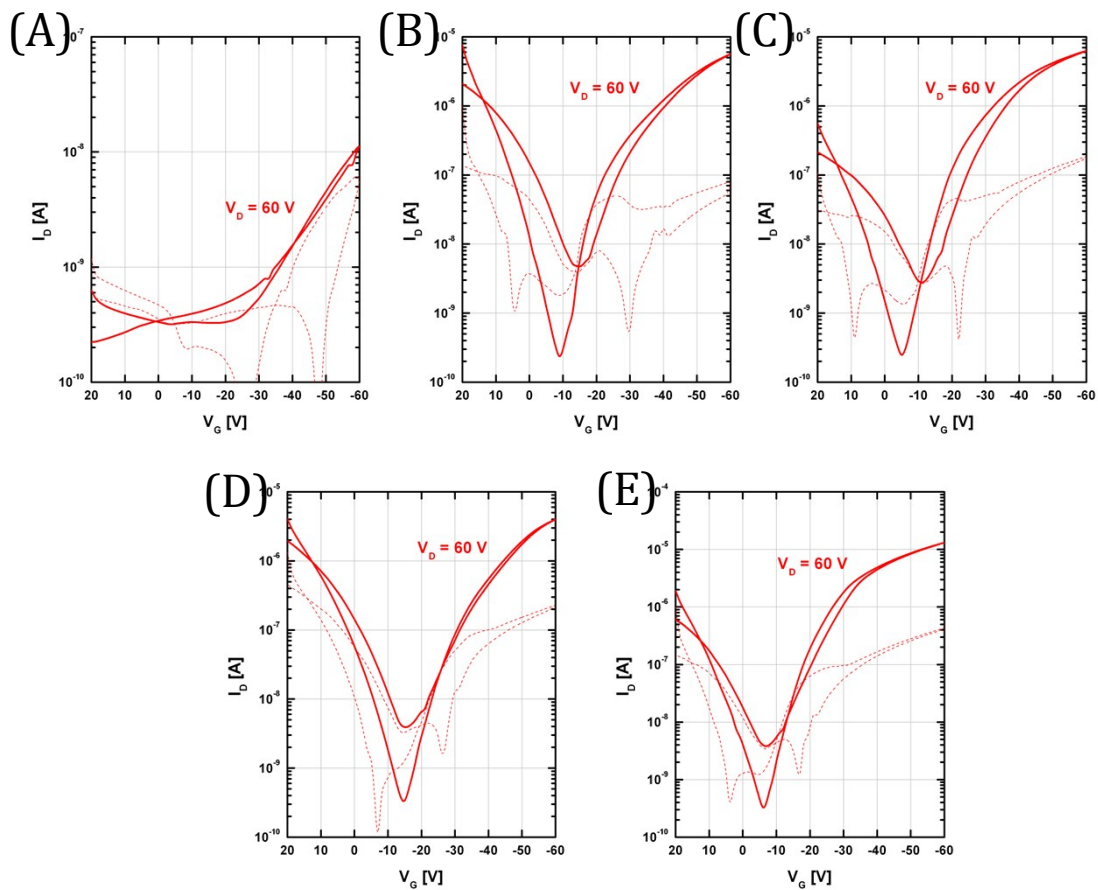


**Figure S5.** Typical transfer plots of neat films of (A) **BDTTDPP**, (B) **BDT(TDPP)<sub>2</sub>**, (C) **BDF(TDPP)<sub>2</sub>**, (D) **NDT(TDPP)<sub>2</sub>**, and (E) **zNDT(TDPP)<sub>2</sub>**

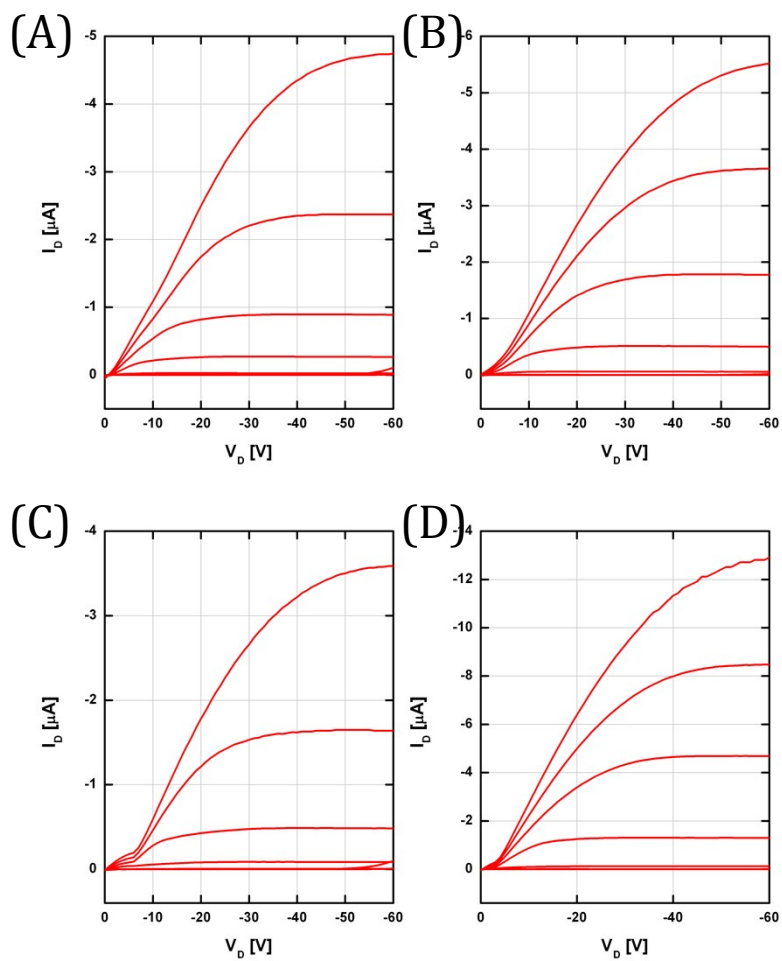


**Figure S6.** Typical output plots of neat films of (A) **BDT**, (B) **BDF**, (C) **NDT**, and (D) **zNDT**

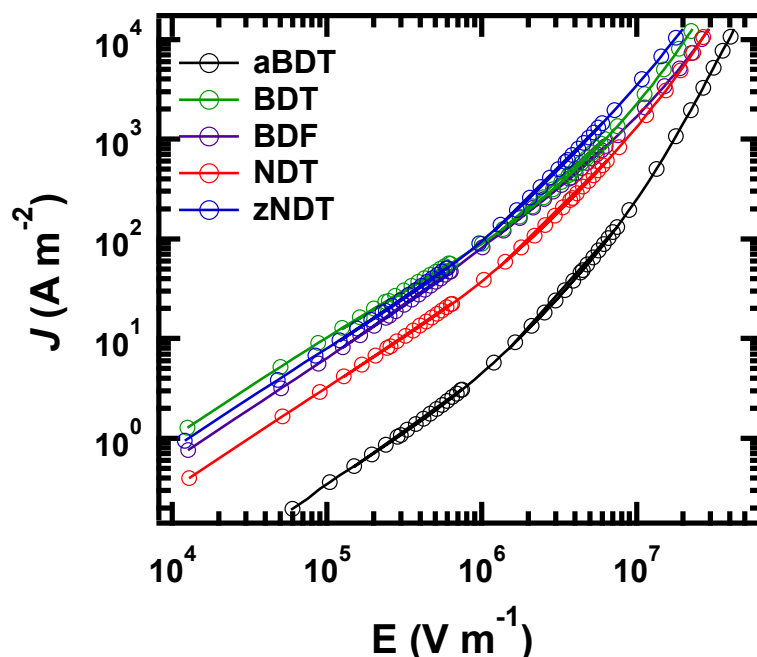


**Figure S7.** J-E response data and fits describing the SCLC mobilities in small molecule donor neat films.

#### *Transmission Electron and Atomic Force Microscopy*

TEM specimens were prepared under identical conditions as the corresponding solar cells using water-soluble PEDOT-PSS as an interfacial layer. After the active layer was spun cast, the PEDOT-PSS film was dissolved and the active layer was floated in DI water, enabling active layer film transfer to a TEM grid and drying before TEM analysis. TEM images were obtained on a Hitachi HD-2300A STEM. AFM active layer samples were analyzed using the same film fabrication conditions used for solar cell device fabrication without deposition of the top electrode. Data collection was performed on a Bruker Dimension ICON PT system in tapping mode with Si-cantilevers.

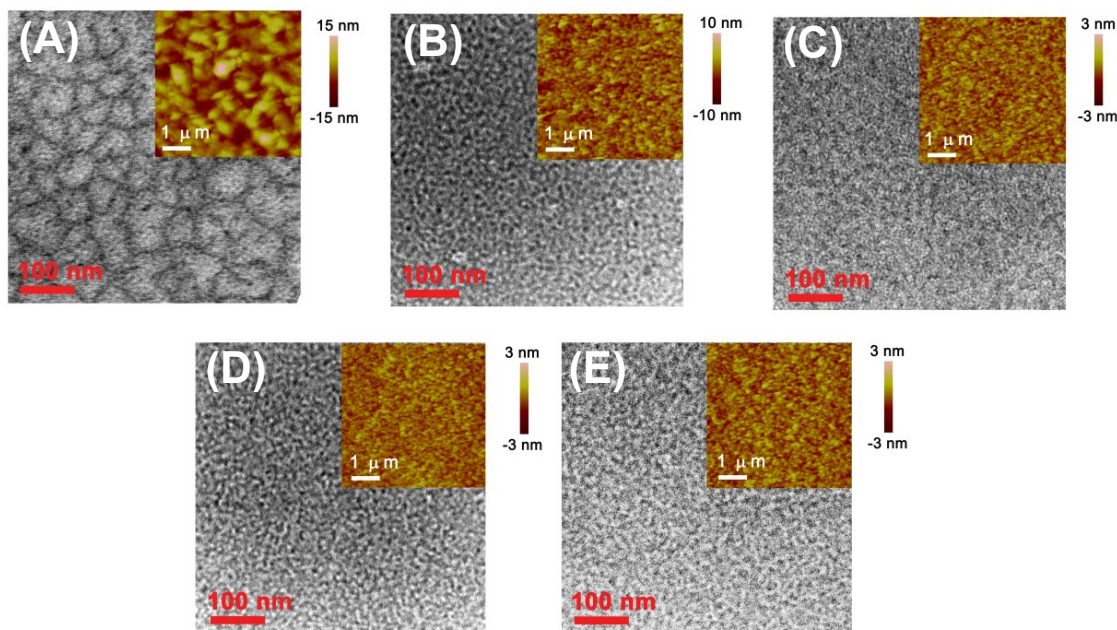


**Figure S8.** Transmission electron and atomic force micrographs (insets) of blend annealed **SM:PCBM** films, (A) **aBDT**, (B) **BDT**, (C) **BDF**, (D) **NDT**, (E) **zNDT**, showing varied domain sizes and roughnesses.

The darker areas are assigned to PCBM domains based on energy dispersive x-ray spectroscopy (EDS) while the lighter areas are primarily small molecule domains. In qualitative agreement with the aforementioned GIXS Scherrer analysis, the **aBDT** films have large, phase separated donor domains, while all A-D-A films all exhibit smaller intermixed domains. The AFM (Figure S8, inset) surface topology closely parallels that observed by TEM. In particular, the **aBDT:PCBM** blend film has the largest domain sizes and the roughest surface (RMS = 3.6 nm), indicating the presence of large **aBDT** crystals.

#### References:

1. S. Loser, C. J. Bruns, H. Miyauchi, R. P. Ortiz, A. Facchetti, S. I. Stupp and T. J. Marks, *J Am Chem Soc*, 2011, **133**, 8142-8145.
2. S. Loser, H. Miyauchi, J. W. Hennek, J. Smith, C. Huang, A. Facchetti and T. J. Marks, *Chem. Commun.*, 2012, **48**, 8511-8513.
3. A. Guerrero, S. Loser, G. Garcia-Belmonte, C. J. Bruns, J. Smith, H. Miyauchi, S. I. Stupp, J. Bisquert and T. J. Marks, *Phys Chem Chem Phys*, 2013, **15**, 16456-16462.

4. D. M. Smilgies, *J Appl Crystallogr*, 2009, **42**, 1030-1034.
5. R. A. Marcus, *Rev Mod Phys*, 1993, **65**, 599-610.
6. J. L. Bredas, D. Beljonne, V. Coropceanu and J. Cornil, *Chem Rev*, 2004, **104**, 4971-5003.
7. Y. Shao, L. F. Molnar, Y. Jung, J. Kussmann, C. Ochsenfeld, S. T. Brown, A. T. B. Gilbert, L. V. Slipchenko, S. V. Levchenko, D. P. O'Neill, R. A. DiStasio, R. C. Lochan, T. Wang, G. J. O. Beran, N. A. Besley, J. M. Herbert, C. Y. Lin, T. Van Voorhis, S. H. Chien, A. Sodt, R. P. Steele, V. A. Rassolov, P. E. Maslen, P. P. Korambath, R. D. Adamson, B. Austin, J. Baker, E. F. C. Byrd, H. Dachsel, R. J. Doerksen, A. Dreuw, B. D. Dunietz, A. D. Dutoi, T. R. Furlani, S. R. Gwaltney, A. Heyden, S. Hirata, C. P. Hsu, G. Kedziora, R. Z. Khalliulin, P. Klunzinger, A. M. Lee, M. S. Lee, W. Liang, I. Lotan, N. Nair, B. Peters, E. I. Proynov, P. A. Pieniazek, Y. M. Rhee, J. Ritchie, E. Rosta, C. D. Sherrill, A. C. Simmonett, J. E. Subotnik, H. L. Woodcock, W. Zhang, A. T. Bell, A. K. Chakraborty, D. M. Chipman, F. J. Keil, A. Warshel, W. J. Hehre, H. F. Schaefer, J. Kong, A. I. Krylov, P. M. W. Gill and M. Head-Gordon, *Phys Chem Chem Phys*, 2006, **8**, 3172-3191.